A Journal of the Gesellschaft Deutscher Chemiker

Angewandte International Edition GDCh Chemie

www.angewandte.org

Accepted Article

Title: Redox ladder of Ni3 complexes with closed-shell, mono-, and diradical triphenylene units: molecular models for conductive 2D MOFs

Authors: Luming Yang and Mircea Dincă

To be cited as: *Angew. Chem. Int. Ed.* 10.1002/anie.202109304

Link to VoR: https://doi.org/10.1002/anie.202109304

WILEY-VCH

10.1002/anie.202109304

WILEY-VCH

RESEARCH ARTICLE

Redox ladder of Ni_3 complexes with closed-shell, mono-, and diradical triphenylene units: molecular models for conductive 2D MOFs

Luming Yang, Mircea Dincă*

[a] L. Yang, Prof. M. Dincă
Department of Chemistry
Massachusetts Institute of Technology
77 Massachusetts Avenue, Cambridge, Massachusetts 02139 (USA)
E-mail: mdinca@mit.edu

Supporting information for this article is given via a link at the end of the document.

Abstract: We report the isolation and characterization of a series of trinickel complexes with 2,3,6,7,10,11-hexaoxotriphenylene (HOTP), $[(Me_3TPANi)_3(HOTP)](BF_4)_n$ (Me_3TPA = *N*,*N*,*N*-tris[(6-methyl-2-pyridyl)methyl]amine) (*n* = 2, 3, 4 for complexes **1**, **2**, **3**). These complexes comprise a redox ladder whereby the HOTP core displays increasingly quinoidal character as its formal oxidation state changes from –4, to –3, and –2 in **1**, **2**, and **3**, respectively. No formal oxidation state changes occur on Ni, allowing the isolation of singlet diradical, monoradical, and closed-shell configurations for HOTP in **1**, **2**, and **3**, respectively, with a concomitant decrease in the spin coupling strength upon oxidation. Because the three complexes can be considered models of the smallest building blocks of 2D conductive metal-organic frameworks such as Ni_9HOTP_4, these results serve as possible inspiration for the construction of extended materials with targeted electric and magnetic properties.

Introduction

Combining high spin density and tunability in chemical composition and electronic structures, electrically conductive two-dimensional metal-organic frameworks (2D MOFs) have soared in interest in part due to potential applications such as spintronics, conductive ferromagnets, and superconductors.[1–8] Many of the electronic features that lead to interesting properties in these materials stem from the ligands, which are most commonly electron-rich molecules derived from a trigonal triphenylene core.[2,9,10] In particular, because the ligands can support multiple redox states that are difficult to control during synthesis, reports rarely provide conclusive evidence for the formal oxidation state or, indeed, even the formula unit of a given MOF.[1,11] Strikingly then, the effect of ligand charge state on the electronic and spin interactions in these materials is still poorly understood.

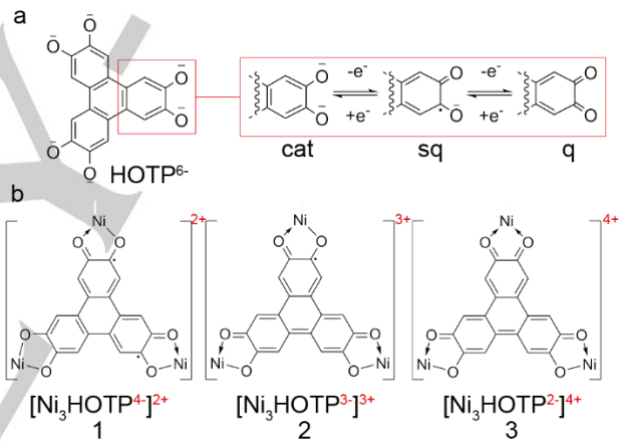

Scheme 1. (a) Lewis structures of $HOTP^{6-}$ and the redox sequence on a catecholate sub-unit; (b) selected resonance structures of 1, 2, and 3, illustrating the charge states and spin structures of $HOTP^{n-}$. Me_3TPA capping ligands are omitted for clarity.

To address this challenge, we aimed to isolate the smallest building unit of a 2D MOF, a trimetallic complex bridged by a single triphenylene ligand, and study its physical properties as a proxy for the extended material. This approach can be envisioned as a dimensional reduction strategy that has proven successful for gaining insight in the electronic structure of extended solids.[12,13] One previous study undertaking this strategy for a Cu-based MOF demonstrated feasibility, but ultimately provided little insight because only a single ligand oxidation state could be isolated and characterized.[14] Here, we isolate model complexes related to the conductive MOF nickel hexaoxytriphenylene (Ni_9HOTP_4)[1,15] in three consecutive oxidation states: $[(Me_3TPANi)_3(HOTP)](BF_4)_n$ (Me_3TPA = *N*,*N*,*N*-tris[(6-methyl-2-pyridyl)methyl]amine) (*n* = 2, 3, 4 for complexes **1**, **2**, **3**), with charge states of –4, –3, and –2, respectively, on the HOTP fragment (Scheme 1b). HOTP serves a particularly attractive target because its three catechol units are, in principle, each capable of engaging in two consecutive one-electron reversible

10.1002/anie.202109304

redox couples in the catecholate-semiquinonate-quinonate (cat-sq-q) sequence (Scheme 1a), affording up to six different oxidation states for a Ni_3HOTP complex. Ni^{2+} is also a rational choice because it exhibits an open-shell electronic structure under octahedral coordination, important for studying spin exchange interactions, but otherwise exhibits redox inert behavior in catecholate complexes.[1,16–20]

Results and Discussion

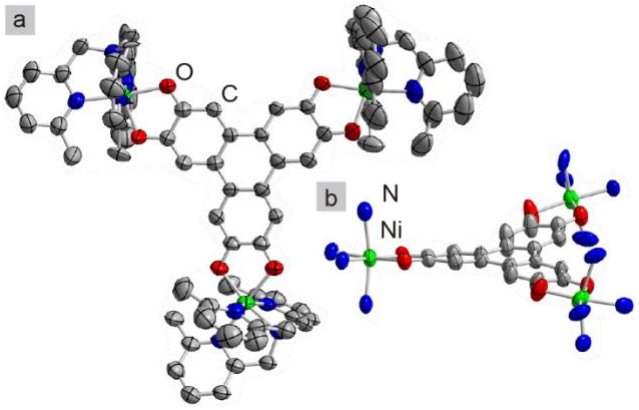

Figure 1. Crystal structure of **2**, showing (a) the cation containing Ni_3HOTP motif and (b) the distortion from planarity of the Ni_3HOTP core. Thermal ellipsoids are plotted at 50% probability level for elements other than hydrogen. Hydrogen atoms and part of the Me_3TPA backbones in (b) are omitted for clarity.

Complexes **2** and **3** were accessed by oxidation of **1** with one equivalent of ferrocenium tetrafluoroborate ($FcBF_4$) or two equivalents of $AgBF_4$ in dichloromethane (DCM) under nitrogen atmosphere (Scheme S1c, d). Complexes **1**, **2**, and **3** were further purified by recrystallization from DCM solutions layered with hexane, giving dark green ribbon-shaped, dark blue needle-shaped, and dark purple needle-shaped crystals, respectively. Although all complexes were analytically pure and crystalline (see Supporting Information, Synthetic Details and Figure S2), only crystals of **2** were of sufficient quality to allow investigation by single crystal X-ray diffraction (XRD). Compound **2** crystallizes in space group $P2_1/n$, with neighboring $[Ni_3HOTP]^{3+}$ moieties well separated in space by Me_3TPA capping each of the Ni^{2+} centers and by three charge-balancing tetrafluoroborate anions (Figure 1a). The average C–O bond length in **2,** 1.28(1) Å, lies close to the reported values for similar trimetallic complexes of $HOTP^{3-}$, and is consistent with all three catecholate groups presenting as semiquinones.[14,19] The average Ni–N bond length of **2**, 2.11(1) Å, is also close to the typical value for Ni^{2+} complexes of Me_3TPA.[20,21] Relevantly, the Ni_3HOTP core deviates from planarity: whereas two Ni^{2+}-semiquinonate sub-units are essentially coplanar, the third catecholate arm twists away from the plane of the first two by 18.9° (Figure 1b). As discussed later, this distortion has important implications for the spin interactions in **2**.

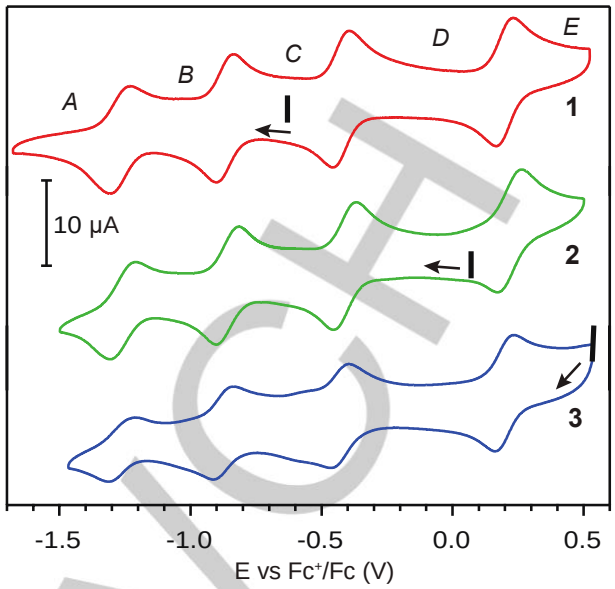

Figure 2. Cyclic voltammograms of **1**, **2**, and **3** measured in 0.2 M solutions of $TBAPF_6$ in DCM under nitrogen. Black marks indicate open circuit potentials. Arrows indicate scanning direction. A, B, C, D, and E mark, respectively, the dominant species within the series $[Ni_3(HOTP^{n-})]^{(6-n)+}$ (n = 6, 5, 4, 3, 2).

Cyclic voltammetry (CV) measurements confirmed the formal charges in each of the complexes. The three complexes share similar CV features, all showing four reversible redox couples at $E_{1/2}$ = –1.31, –0.90, –0.46, and +0.18 V with respect to the ferrocenium/ferrocene (Fc^+/Fc) couple (Figure 2). We assign these to ligand-center redox events: $HOTP^{5-/6-}$, $HOTP^{4-/5-}$, $HOTP^{3-/4-}$, and $HOTP^{2-/3-}$, respectively, in line with literature reports for similar systems.[14,19,22,23] The CVs for complexes **1-3** differ only in their open-circuit potential (OCP), measured at –0.63, +0.05, and +0.54 V vs. Fc^+/Fc for **1**, **2**, and **3**, respectively. These OCP values confirm that the HOTP moieties in **1**, **2**, and **3** carry formal charges of –4, –3, and –2, respectively, as described in Scheme 1. The electrochemical data, taken in the context of classical mixed-valence theory and considering each HOTP moiety as being composed of three catecholate subunits, offers an important clue into the degree of electron delocalization within the HOTP ligand. In particular the difference of 0.64 V between the $E_{1/2}$ potentials of the $HOTP^{3-/4-}$ and $HOTP^{2-/3-}$ redox couples equates to a comproportionation constant K_c of $10^{10.8}$ (see Figure S3 and related discussion).This corresponds to full delocalization among the three semiquinonate sub-units, allowing the classification of **2** as a Robin-Day class III mixed-valence compound.[14,24–26] The increased oxidation of the ligand in going from **1** to **2** and **3** was also evidenced spectroscopically: in the UV-Visible-near-IR region, a blue-shift of the lowest energy absorption was observed from **1**, to **2**, to **3**, with the peak maximum shifting from 1386, to 1196, and 1114 nm (all with $\epsilon \sim 10^4$ $M^{-1}cm^{-1}$) (Figure S6a). A blue-shift of the lowest-energy absorption in the near-IR region has been associated with an increase of quinoidal character in related trinuclear HOTP complexes.[27] In the mid-IR region, a blue-shift of the ν(C–O)-based stretching band from 1310, 1331, to 1341 cm^{-1}, again suggests increased quinoidal character and C–O bond order in HOTP upon oxidation from **1** to **2** and **3** (Figure S7).[28] Altogether, CV and UV-Visible-IR measurements confirm **1**, **2**, and **3** as a

10.1002/anie.202109304

redox ladder of three successive oxidation states for $[Ni_3(HOTP)]^{n+}$ (n = 2, 3, and 4) with electron transfer events all ligand-based.

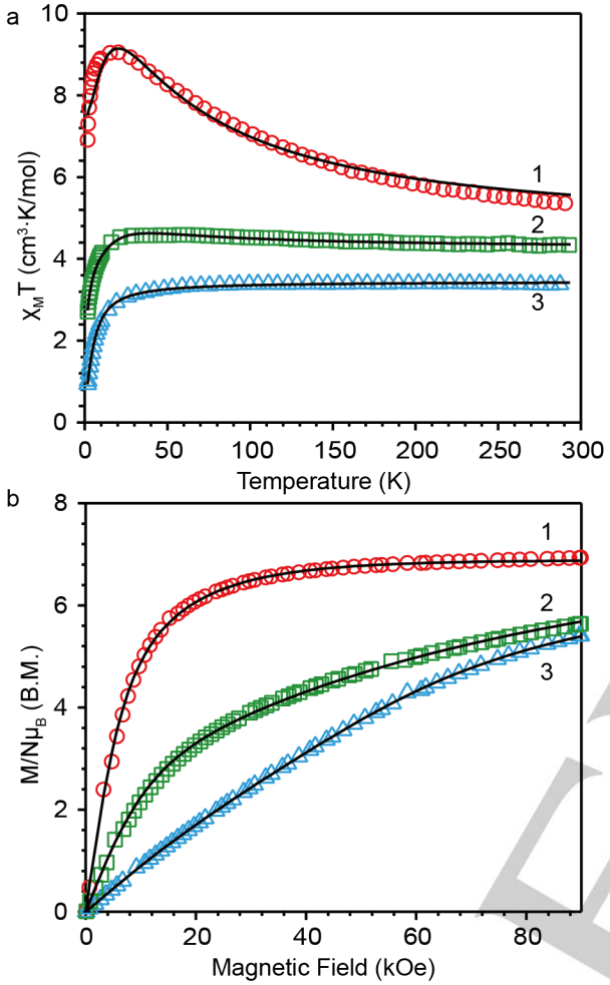

Figure 3. (a) Temperature-dependent $\chi_M T$ (H = 1.0 kOe) and (b) field-dependent magnetization (T = 1.8 K) curves for **1**, **2**, and **3**. The solid black lines are fits described in the text.

Magnetometry measurements provided critical insight into the nature and strength of spin coupling in the three complexes. Variable temperature direct current susceptibility measurements revealed that the $\chi_M T$ of **1** increases significantly from 5.36 cm^{3}mol^{-1}K at 293 K to a maximum of 9.04 cm^{3}mol^{-1}K at 15 K, before a sharp drop to 6.91 cm^{3}mol^{-1}K at 1.8 K (Figure 3a). This behavior is indicative of strong ferromagnetic interactions within **1**. A variable field magnetization measurement of **1** at 1.8 K reveals early saturation above 20 kOe to a reduced magnetization value of 6.94 B.M. (Figure 3b). A reasonable first thought for interpreting this data is to model **1** as a three-spin system with a closed-shell $HOTP^{4-}$ ligand connecting three octahedral S = 1 Ni^{2+} centers. Under this assumption, the highest possible spin value for **1** would be S = 3, if the three Ni^{2+} centers are coupled ferromagnetically (Figure S8c). This would give a saturation magnetization of 6.94 B.M. and a corresponding g-value of ~2.3. The latter value is further supported by the variable-temperature-variable-field (VTVH) magnetization data for **1** in the temperature range 1.8-10 K under magnetic fields of 10-70 kOe (see Figure S9 and related discussion). However, this model would give a maximum value of $\chi_M T$ ~7.9 cm^{3}mol^{-1}K, significantly lower than the observed $\chi_M T$ maximum of 9.04 cm^{3}mol^{-1}K. Forcing $HOTP^{4-}$ to remain closed-shell while fitting the $\chi_M T$ data leads to an unreasonably high isotropic g-value of 2.45 for Ni^{2+}, in further disagreement with the VTVH data (Figure S10 and related discussion).

Intriguingly, an alternative model for the spin structure of **1** assumes that $HOTP^{4-}$ possesses diradical character instead of a closed-shell configuration. This diradical formalism is not unprecedented for hexa-substituted triphenylene moieties in the 4– redox state.[29,30] It involves two coupled HOTP-centered S = 1/2 radicals, each further coupled to the three S = 1 Ni^{2+} centers (Figure S8a). The $\chi_M T$ and reduced magnetization data can be fit to this model using a Hamiltonian with the following terms describing the isotropic exchange coupling [Eq. (1)]:

$$\mathcal{H}_1 = \mathcal{H}_{11} + \mathcal{H}_{12} + \mathcal{H}_{13}; \quad (1)$$

$$\mathcal{H}_{11} = -2J_1(\boldsymbol{S}_{Ni_1}\boldsymbol{S}_{Ni_2} + \boldsymbol{S}_{Ni_1}\boldsymbol{S}_{Ni_3} + \boldsymbol{S}_{Ni_2}\boldsymbol{S}_{Ni_3}); \quad (2)$$

$$\mathcal{H}_{12} = -(2J_2 \sum_{i=1,2,3} \boldsymbol{S}_{Ni_i}\boldsymbol{S}_L + 2J_3 \sum_{i=1,2,3} \boldsymbol{S}_{Ni_i}\boldsymbol{S}_L); \quad (3)$$

$$\mathcal{H}_{13} = -2J_4\boldsymbol{S}_{L1}\boldsymbol{S}_{L2}; \quad (4)$$

where $\mathcal{H}_{11}$ [Eq. (2)], $\mathcal{H}_{12}$ [Eq. (3)], and $\mathcal{H}_{13}$ [Eq. (4)] describe the Ni^{2+}-Ni^{2+}, Ni^{2+}-radical, and radical-radical spin interactions. Good fits were obtained for J_1 = +7.0 cm^{-1}, J_2 = +16.8 cm^{-1}, J_3 = +22.8 cm^{-1}, J_4 = –64.0 cm^{-1}, g_{Ni} = 2.28, and $|D_{Ni}|$ = 2.0 cm^{-1}, with g_{HOTP} fixed to the free electron value of 2.0 (Figure 3). The competing ferromagnetic and antiferromagnetic interactions between the Ni^{2+}-Ni^{2+}, Ni^{2+}-radical, and radical-radical pairs produce a S = 3 spin ground state for **1**, in line with the value expected from the magnetization data. Expectedly, the strongest exchange interaction takes place within the HOTP moiety, where the geometric distortion away from planarity likely determines the antiferromagnetic coupling of the two radicals. The ferromagnetic Ni^{2+}-radical interactions are in line with previous observations in Ni^{2+}-semiquinonate complexes, and can be explained by the orthogonality of the Ni^{2+} and $HOTP^{4-}$ magnetic orbitals.[18,31]

Parallel and perpendicular X-band electron paramagnetic resonance (EPR) spectroscopy provided further validation for the electronic structure of the complexes. At 4.5 K, frozen glasses of DCM solutions of **2** gave an intense signal with g = 15.14 and a weaker signal with g = 2.31, both only observed under parallel mode (Figure 4). These features are assigned to the transition within the m_s = ±3 and m_s = ±1 doublets of the S = 3 ground state upon further introducing rhombicity to the Ni^{2+}-centered spins. Indeed, the two main EPR features were reproduced by a simulation with the above fitting parameters and an E/D = 0.12 (Figure 4a, black trace), without losing the quality of fit of the magnetometry data (Figure S11). The consistency of magnetometry and EPR data supports our assignment of the spin structure of **1**, namely an unusual open-shell singlet diradical on $HOTP^{4-}$.

The $\chi_M T$ of **2** exhibits a slight increase from 4.35 cm^{3}mol^{-1}K at 293 K to a maximum of 4.62 cm^{3}mol^{-1}K near 25 K, suggesting a weak overall ferromagnetic interaction between Ni^{2+} centers (Figure 3a). Below 25 K, $\chi_M T$ dropped abruptly to 2.73 cm^{3}mol^{-1}K at 1.8 K, typical for octahedral Ni^{2+}-centered spins with zero-field

10.1002/anie.202109304

splitting. The presence of zero-field splitting also agrees with the absence of saturation up to 90 kOe in the saturation magnetization measurement (Figure 3b). Based on these data, **2** should have three Ni^{2+}-centered S = 1 spins and a $HOTP^{3-}$-centered S = 1/2 spin. Although $\chi_M T$ at 293 K is higher than the expected value for such a model (3.38 $cm^3mol^{-1}K$ with g = 2.0), octahedral Ni^{2+} centers often exhibit g-values larger than 2.0.[32,33] Indeed, fitting the $\chi_M T$ and reduced magnetization data for **2** to a straightforward Hamiltonian:

$$\mathcal{H}_2 = -2J_1\boldsymbol{S}_{Ni_1}\boldsymbol{S}_{HOTP} - 2J_2(\boldsymbol{S}_{Ni_2}\boldsymbol{S}_{HOTP} + \boldsymbol{S}_{Ni_3}\boldsymbol{S}_{HOTP}) \quad (5)$$

where two g, J, and D are used to account for the low symmetry observed in the crystal structure (see Figure S8b and related discussions) gave good fits for J_1 = –6.4 cm^{-1} and J_2 = +12.5 cm^{-1} ($g_1 = g_2$ = 2.28, $|D_1|$ = 21.5 cm^{-1}, $|D_2|$ = 5.7 cm^{-1}) and an overall spin ground state S = 3/2 [Eq. (5)].

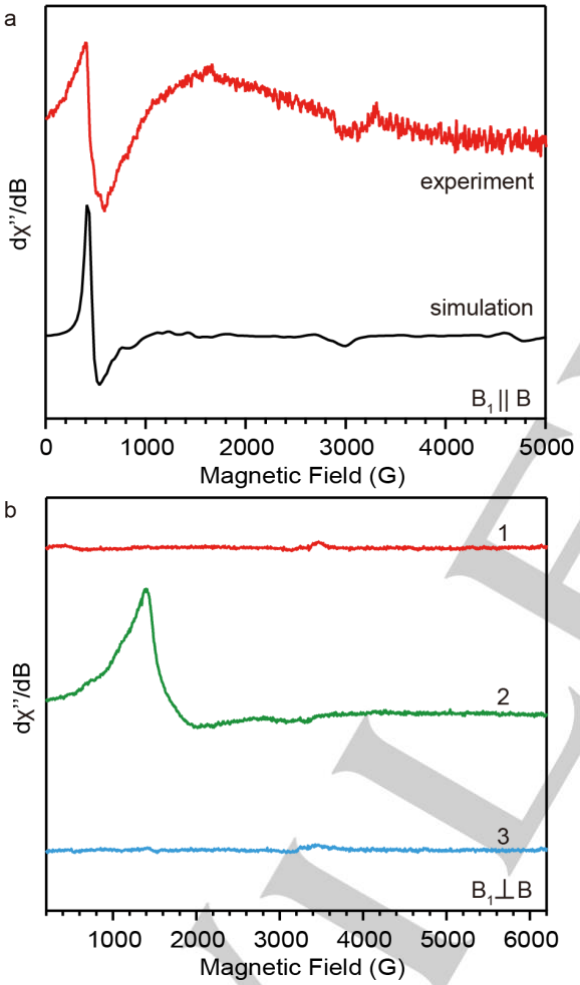

Figure 4. (a) Experimental and simulated EPR spectra for **1** under parallel mode; (b) experimental EPR spectra for **1**, **2**, **3** under perpendicular mode. All measurements were carried out at 4.5 K.

Perpendicular-mode EPR measurements corroborate these fit parameters: at 4.5 K, the spectrum of **2** displayed an intense positive peak with a maximum at 1390 G (g = 4.82) and a broad negative peak with a minimum at around 2050 G (g = 3.27) (Figure 4b). Upon increasing the temperature to 45 K, the overall intensity of the signal decreased, with an increase of relative intensity in the range of 520-1150 G (g ~ 12.8-5.8) to that at 1390 G (Figure S12). This temperature dependence is expected for a system described by the above fitting parameters, where thermal excitation from the S = 3/2 ground state with $g_\perp$ = 2.21 and $g_\parallel$ = 4.94 leads to population of low-lying spin excited states with g-values ranging from 5.77 to 11.22 (Table S2).

Finally, the $\chi_M T$ of **3** decreased gradually with temperature from 3.38 $cm^3mol^{-1}K$ at 293 K to 3.08 $cm^3mol^{-1}K$ near 30 K, followed by a sharp decrease to 0.93 $cm^3mol^{-1}K$ at 1.8 K (Figure 3a). This temperature dependence, together with the absence of magnetic saturation up to 90 kOe at 1.8 K (Figure 3b), suggests the presence of overall weak antiferromagnetic interactions between the Ni^{2+}-centered S = 1 spins and zero-field splitting at the Ni^{2+} centers. The $\chi_M T$ value at 293 K agrees well with the predicted value for three uncoupled S = 1 spins (3.0 $cm^3mol^{-1}K$ with g = 2.0). Fitting the magnetometry data to the exchange Hamiltonian:

$$\mathcal{H}_3 = -2J_1\boldsymbol{S}_{Ni_2}\boldsymbol{S}_{Ni_3} - 2J_2(\boldsymbol{S}_{Ni_1}\boldsymbol{S}_{Ni_2} + \boldsymbol{S}_{Ni_1}\boldsymbol{S}_{Ni_3}) \quad (6)$$

gave best fit parameters J_1 = –0.4 cm^{-1} and J_2 = –0.9 cm^{-1} (g_1 = 2.05, $|D_1|$ = 2.6 cm^{-1}; g_2 = 2.19, $|D_2|$ = 1.2 cm^{-1}; Figure S8c) [Eq. (6)]. These parameters correspond to two weak antiferromagnetic pathways with slightly unequal strength, giving rise to a spin ground state of S = 1. Compound **3** remains EPR-silent in both perpendicular and parallel modes at X-band (Figure 4).

Conclusion

Altogether, structural, electrochemical, spectroscopic, and magnetic data support the increase of HOTP oxidation state and progressive quinoidal character from **1** to **3**. The electron density on HOTP delocalizes significantly for all HOTP charge states, and is in line with the observed excellent charge delocalization in MOFs made with the same ligand.[15,34] Indeed, the comproportionation constant describing HOTP-based redox events is among the largest for complexes with triphenylene bridges.[14,19,22,23,27] In the three trinuclear nickel complexes reported here, the HOTP moieties take spin configurations of singlet diradical, monoradical, and closed-shell as they become doubly, triply, or quadruply oxidized relative to the fully reduced $HOTP^{6-}$. Importantly, the spin coupling strength decreases as HOTP becomes more oxidized, likely due to the decrease in the spin density on this bridging ligand.[35–37] Notably, **1** is a rare example of diradical delocalized π-type bridging ligand. Here, its diradical nature is likely stabilized by the coordination to electron-withdrawing metal cations, by mixing with low-lying excited electronic states,[38–40] and not least by its singlet ground state, likely stemming from the distortion from coplanarity.[41,42] In fact, **1** represents the first isolated example of a diradical triphenylene bridge, the closest previous example a triiron complex characterized only in solution and never isolated. Compounds **1** and **2** further serve as rare examples of complexes containing tritopic radical bridges, an important motif that is challenging to achieve in molecular-based magnetic materials.[37,43,44]

Radical ligands have attracted considerable attention recently as potential building blocks for molecular and extended magnetic molecules and materials.[37,43,44] Our report therefore provides additional rationale for using HOTP and other triphenylene linkers as precursors for such targets. Finally, the distortion of the triphenylene core and its critical influence on the magnetic

10.1002/anie.202109304

exchange couplings provides new ideas for targeting extended materials, including 2D MOFs, made from distorted cores that may exhibit strong magnetic interactions and bulk magnetism, a current direction of interest in our laboratory.

Deposition Number 2095320 contains the supplementary crystallographic data for this paper. The data is provided free of charge by the Cambridge Crystallographic Data Center.

Acknowledgements

This work was supported by the National Science Foundation (Waterman Award to MD; DMR-1645232). We thank Dr. G. Skorupskii and Dr. L. S. Xie for assistance with crystallography, and Dr. H. Banda for insightful discussions regarding electrochemistry.

Keywords: Radicals • Bridging ligands • Magnetism • Redox chemistry • Metal-organic frameworks

[1] M. Hmadeh, Z. Lu, Z. Liu, F. Gándara, H. Furukawa, S. Wan, V. Augustyn, R. Chang, L. Liao, F. Zhou, E. Perre, V. Ozolins, K. Suenaga, X. Duan, B. Dunn, Y. Yamamto, O. Terasaki, O. M. Yaghi, *Chem. Mater.* **2012**, *24*, 3511–3513.

[2] D. Sheberla, L. Sun, M. A. Blood-Forsythe, S. Er, C. R. Wade, C. K. Brozek, A. Aspuru-Guzik, M. Dincă, *J. Am. Chem. Soc.* **2014**, *136*, 8859–8862.

[3] J. H. Dou, L. Sun, Y. Ge, W. Li, C. H. Hendon, J. Li, S. Gul, J. Yano, E. A. Stach, M. Dincă, *J. Am. Chem. Soc.* **2017**, *139*, 13608–13611.

[4] X. Song, X. Wang, Y. Li, C. Zheng, B. Zhang, C. Di, F. Li, C. Jin, W. Mi, L. Chen, W. Hu, *Angew. Chem., Int. Ed.* **2020**, *59*, 1118–1123.

[5] R. Dong, Z. Zhang, D. C. Tranca, S. Zhou, M. Wang, P. Adler, Z. Liao, F. Liu, Y. Sun, W. Shi, Z. Zhang, E. Zschech, S. C. B. Mannsfeld, C. Felser, X. Feng, *Nat. Commun.* **2018**, *9*, 2637.

[6] X. Huang, S. Zhang, L. Liu, L. Yu, G. Chen, W. Xu, D. Zhu, *Angew. Chem., Int. Ed.* **2018**, *57*, 146–150.

[7] M. Ko, L. Mendecki, K. A. Mirica, *Chem. Commun.* **2018**, *54*, 7873–7891.

[8] C. Yang, R. Dong, M. Wang, P. S. Petkov, Z. Zhang, M. Wang, P. Han, M. Ballabio, S. A. Bräuninger, Z. Liao, J. Zhang, F. Schwotzer, E. Zschech, H. H. Klauss, E. Cánovas, S. Kaskel, M. Bonn, S. Zhou, T. Heine, X. Feng, *Nat. Commun.* **2019**, *10*, 1–9.

[9] L. Sun, M. G. Campbell, M. Dincă, *Angew. Chem., Int. Ed.* **2016**, *55*, 3566–3579.

[10] T. Kambe, R. Sakamoto, K. Hoshiko, K. Takada, M. Miyachi, J. H. Ryu, S. Sasaki, J. Kim, K. Nakazato, M. Takata, H. Nishihara, *J. Am. Chem. Soc.* **2013**, *135*, 2462–2465.

[11] D. Feng, T. Lei, M. R. Lukatskaya, J. Park, Z. Huang, M. Lee, L. Shaw, S. Chen, A. A. Yakovenko, A. Kulkarni, J. Xiao, K. Fredrickson, J. B. Tok, X. Zou, Y. Cui, Z. Bao, *Nat. Energy* **2018**, *3*, 30–36.

[12] J. R. Long, A. S. Williamson, R. H. Holm, *Angew. Chem., Int. Ed.* **1995**, *34*, 226–229.

[13] J. L. Heinrich, P. A. Berseth, J. R. Long, *Chem. Commun.* **1998**, *4*, 1231–1232.

[14] L. Yang, X. He, M. Dincă, *J. Am. Chem. Soc.* **2019**, *141*, 10475–10480.

[15] D. G. Ha, M. Rezaee, Y. Han, S. A. Siddiqui, R. W. Day, L. S. Xie, B. J. Modtland, D. A. Muller, J. Kong, P. Kim, M. Dincă, M. A. Baldo, *ACS Cent. Sci.* **2021**, *7*, 104–109.

[16] C. G. Pierpont, L. C. Francesconi, D. N. Hendrickson, *Inorg. Chem.* **1977**, *16*, 2367–2376.

[17] C. Brückner, D. L. Caulder, K. N. Raymond, *Inorg. Chem.* **1998**, *37*, 6759–6764.

[18] M. Bubnov, A. Cherkasova, I. Teplova, E. Kopylova, G. Fukin, M. Samsonov, A. Bogomyakov, S. Fokin, G. Romanenko, V. Cherkasov, V. Ovcharenko, *Polyhedron* **2016**, *119*, 317–324.

[19] Y. Wang, F. Lambert, E. Rivière, R. Guillot, C. Herrero, A. Tissot, Z. Halime, T. Mallah, *Chem. Commun.* **2019**, *55*, 12336–12339.

[20] K. Shiren, S. Ogo, S. Fujinami, H. Hayashi, M. Suzuki, A. Uehara, Y. Watanabe, Y. Moro-oka, *J. Am. Chem. Soc.* **2000**, *122*, 254–262.

[21] P. Halder, B. Chakraborty, P. R. Banerjee, E. Zangrando, T. K. Paine, *CrystEngComm* **2009**, *11*, 2650–2659.

[22] A. M. Barthram, Z. R. Reeves, J. C. Jeffery, M. D. Ward, *J. Chem. Soc. Dalt. Trans.* **2000**, 3162–3169.

[23] L. R. Dalesio, J. O. Hill, M. Kraimer, S. Lewis, D. Murray, S. Hunt, W. Watson, M. Clausen, J. Dalesio, *Nucl. Instruments Methods Phys. Res. Sect. A Accel. Spectrometers, Detect. Assoc. Equip.* **1994**, *352*, 179–184.

[24] D. E. Richardson, H. Taube, *Coord. Chem. Rev.* **1984**, *60*, 107–129.

[25] R. Sakamoto, T. Kambe, S. Tsukada, K. Takada, K. Hoshiko, Y. Kitagawa, M. Okumura, H. Nishihara, *Inorg. Chem.* **2013**, *52*, 7411–7416.

[26] M. B. Robin, P. Day, **1968**, pp. 247–422.

[27] C. S. Grange, A. J. H. M. Meijer, M. D. Ward, *Dalt. Trans.* **2010**, *39*, 200–211.

[28] T. T. Patricia, M. V. Sandra, L. Manuela, L. Andrea, F. Paolo, D. Andrea, R. Roberto, *Phys. Chem. Chem. Phys.* **2012**, *14*, 1038–1047.

[29] K. Bechgaard, V. D. Parker, *J. Am. Chem. Soc.* **1972**, *94*, 4749–4750.

[30] N. Hoshino, T. Akutagawa, *Chem. – A Eur. J.* **2018**, *24*, 19323–19331.

[31] C. Benelli, A. Dei, D. Gatteschi, L. Pardi, *Inorg. Chem.* **1988**, *27*, 2831–2836.

[32] O. Kahn, *Molecular Magnetism*, VCH Publishers, Inc., **1993**.

[33] G. Novitchi, S. Jiang, S. Shova, F. Rida, I. Hlavička, M. Orlita, W. Wernsdorfer, R. Hamze, C. Martins, N. Suaud, N. Guihéry, A. L. Barra, C. Train, *Inorg. Chem.* **2017**, *56*, 14809–14822.

[34] R. W. Day, D. K. Bediako, M. Rezaee, L. R. Parent, G. Skorupskii, M. Q. Arguilla, C. H. Hendon, I. Stassen, N. C. Gianneschi, P. Kim, M. Dincă, *ACS Cent. Sci.* **2019**, *5*, 1959–1964.

[35] J. D. Rinehart, M. Fang, W. J. Evans, J. R. Long, **2011**, *3*, DOI 10.1038/nchem.1063.

[36] J. O. Moilanen, N. F. Chilton, B. M. Day, T. Pugh, R. A. Layfield, *Angew. Chem., Int. Ed.* **2016**, *55*, 5521–5525.

[37] S. Demir, I.-R. Jeon, J. R. Long, T. D. Harris, *Coord. Chem. Rev.* **2015**, *289–290*, 149–176.

[38] W. Wang, L. Ge, G. Xue, F. Miao, P. Chen, H. Chen, Y. Lin, Y. Ni, J. Xiong, Y. Hu, J. Wu, Y. Zheng, *Chem. Commun.* **2020**, *56*, 1405–1408.

[39] K. Kamada, K. Ohta, A. Shimizu, T. Kubo, R. Kishi, H. Takahashi, E. Botek, B. Champagne, M. Nakano, *J. Phys. Chem. Lett.* **2010**, *1*, 937–940.

[40] T. Stuyver, B. Chen, T. Zeng, P. Geerlings, F. De Proft, R. Hoffmann, *Chem. Rev.* **2019**, *119*, 11291–11351.
[41] M. Abe, *Chem. Rev.* **2013**, *113*, 7011–7088.
[42] D. A. Shultz, R. M. Fico, S. H. Bodnar, R. K. Kumar, K. E. Vostrikova, J. W. Kampf, P. D. Boyle, *J. Am. Chem. Soc.* **2003**, *125*, 11761–11771.
[43] T. B. Faust, D. M. D'Alessandro, *RSC Adv.* **2014**, *4*, 17498–17512.
[44] A. E. Thorarinsdottir, T. D. Harris, *Chem. Rev.* **2020**, *120*, 8716–8789.

10.1002/anie.202109304

Entry for the Table of Contents

Insert graphic for Table of Contents here.

TRIGONAL TRINICKEL CLUSTER

The article investigates spin coupling and electronic delocalization in trinickel clusters bridged by the radical-containing tritopic ligand 2,3,6,7,10,11-hexaoxytriphenylene (HOTP). The HOTP spin state and strength of Ni-HOTP magnetic coupling can be tuned by consecutive HOTP-centered redox processes. The results provide inspiration for the design of new molecular and solid-state magnetic and electrically conductive materials.

Institute and/or researcher Twitter usernames: @DincaGroupMIT @ChemistryMIT